

The Role of Snow on Microwave Emission and Scattering over First-Year Sea Ice

David G. Barber, A. K. Fung, *Fellow, IEEE*, Thomas C. Grenfell, *Associate Member, IEEE*,
 Son V. Nghiem, *Member, IEEE*, Robert G. Onstott, *Member, IEEE*, V. I. Lytle, *Member, IEEE*,
 Donald K. Perovich, and Anthony J. Gow

Abstract—The primary objective of this paper is to investigate the geophysical and thermodynamic effects of snow on sea ice in defining the electromagnetic (EM) interaction within the microwave portion of the spectrum. We combine observational evidence of both the physical and thermodynamic characteristics of snow with direct measurements of scattering and emission at a variety of frequencies. We explain our observational results using various “state-of-the-art” forward scattering and emission models.

Results show that geophysical characteristics of snow effect emission above about 37 GHz and above 5 GHz for active microwave scattering. We understand these effects to be driven by grain size and its contribution to volume scattering in both passive and active interactions within the volume. With snow cover, the Brewster angle effect is not significant and there is a gradual rise in emission from 10 to 37 GHz. We find emissivity to be dominated by direct emission from saline ice through the snow layer. Hence, the influence of grain size is small but the trend is clearly a drop in total emission as the grain size increases. We find that the role of the volume fraction of snow on emission and scattering is a complex relationship between the number density of scatterers relative to the coherence of this scattering ensemble. At low volume fractions, we find that independent scattering dominates, resulting in an increase in albedo and the extinction coefficient of the snow with frequency.

The thermodynamic effects of snow on microwave scattering and emission are driven by the role that thermal diffusivity and conductivity play in the definition of brine volumes at the ice surface and within the snow volume. Prior to the presence of water in liquid phase within the snow volume, we find that the indirect effects are dominated by an impedance matching process across the snow–ice interface. We find that the complex permittivity at the snow–ice interface is considerably higher than over the bare ice surface. Our results showed that only a small change occurs between the cold and warm cases at lower frequencies, but as expected, the change in emissivity is larger at higher frequencies. Once water in liquid phase appears within

the snow cover, we find that both emission and scattering are directly affected by the high complex permittivity of this volume fraction within the snow layer.

I. INTRODUCTION

SNOW cover on sea ice plays a central role in the exchange of mass and energy across the ocean–sea ice–atmosphere interface. Because of the high albedo of snow, the shortwave radiative exchanges dominate the sea ice–albedo feedback mechanism. Ecologically, this dominance is manifested in a narrow range of photosynthetically active radiation (PAR) available to subice primary producers. Evolutionary adaptation by these organisms illustrates that the marine cryosphere physical system operates within a narrow range of geophysical and energy balance conditions to support the associated biological system. When the physical system evolves outside of these bounds, ecological consequences occur throughout the trophic structure of the marine food chain. Thermodynamically, snow plays a central role in the accretion and ablation of sea ice because of its relatively small thermal conductivity. The amount and timing of snow depositional events appears to have significant consequences on the equilibrium thermodynamics of the sea ice and the rate of accretion and ablation [1].

The radiative and thermodynamic properties of snow become important in the context of climate change scenarios. Projections for climate warming indicate that the polar regions may provide both a larger magnitude and earlier indication of climate variability and change than will the more temperate regions of the planet. Significant uncertainty exists in our understanding of the fundamental role that snow cover plays in the overall energy balance of the marine cryosphere. For example, various modeling and empirical studies provide contradictory evidence as to the sign and magnitude of the sea ice–albedo feedback mechanism because of the uncertainties associated with the role of snow in this process (see [1]–[4] and others).

At both poles information on snow is scarce. This is because of the inherent difficulties in measuring snow distributions remotely and/or the density and representativeness of climate reporting stations. Historical data on snow thickness distributions and their relationship to types of sea ice are also rare. Models of snow thermodynamic, dynamic, and radiative transfer are in their infancy, particularly when considered within the sea ice context.

Electromagnetic (EM) interactions over a broad spectrum hold potential as a means of developing approaches to remotely estimating both the magnitude (depth and/or snow

Manuscript received October 31, 1997; revised June 19, 1998. This work was supported by the Office of Naval Research through the Sea Ice Electromagnetics Accelerate Research Initiative, under Grant N00014-94-1-03-86. The work of D. G. Barber was supported by a Natural Sciences and Engineering Research Council (NSERC) Grant.

D. G. Barber is with the Department of Geography, University of Manitoba, Winnipeg, Man., R3T2N2 Canada (e-mail: dbarber@ms.umanitoba.ca).

A. K. Fung is with the Electrical Engineering Department, University of Texas, Arlington, TX 76019 USA.

T. C. Grenfell is with the Department of Atmospheric Sciences, University of Washington, Seattle, WA 98195 USA.

S. V. Nghiem is with the Jet Propulsion Laboratory, California Institute of Technology, Pasadena, CA 91109 USA.

R. G. Onstott is with the Environmental Research Institute of Michigan, Ann Arbor, MI 48107 USA.

V. I. Lytle is with Antarctic CRC and Australian Antarctic Division, 7001 Tasmania, Australia.

D. K. Perovich and A. J. Gow are with the U.S. Army Cold Regions Research and Engineering Laboratory, Hanover, NH 03755 USA.

Publisher Item Identifier S 0196-2892(98)06663-7.

water equivalence) and spatial pattern of snow on sea ice. The Office of Naval Research (ONR) Electromagnetics Accelerated Research Initiative (ARI) provided a unique opportunity to gather members of the geophysical, modeling and EM communities to evolve our understanding of how various frequencies of EM energy interact with snow on first-year sea ice. The laboratory experiments at the United States Army Cold Regions Research and Engineering Laboratory, Hanover, NH, (CRRELEX) and the field experiments at Point Barrow, AK, and the Canadian high Arctic provide complementary observational data and have been used in combination to initialize forward models to help us understand the primary mechanisms responsible for the geophysical and thermodynamic effects of snow on microwave scattering and emission.

A. Background

Conceptually, snow can affect EM interactions either through direct scattering due to the number density and geophysical characteristics of the snow volume (e.g., density, salinity, grain size, and shape) and through the thermodynamic control on the dielectric properties of snow (e.g., brine volume). In this paper, we attempt to separate geophysical and thermodynamic effects with the caveat that in natural snow covers these two components are highly coupled. In the visible and the near infrared (NIR), the snow cover dominates the radiative transfer throughout the annual cycle of sea ice accretion and ablation [5]. In the microwave portion of the spectrum, results have shown that emission from the surface is directly controlled by the evolution of grain size, density, and water in liquid phase [6]. Microwave scattering appears to be directly effected by the snow cover when water in liquid phase is present (see [6]–[8] and others). Thermodynamic effects have been observed when the brine volume in the basal layer of the snow cover responds to atmospheric and/or oceanic forcing [9].

Laboratory studies [10], [11] of smooth ice sheets with and without a snow cover have found that a thin layer of snow changed the backscatter at microwave frequencies. The backscatter over smooth, bare ice and smooth, snow-covered ice was measured at Ku-Band [10], [11] and C-Band [11] by using step-frequency microwave radars. These studies found that even a thin snow cover (2 cm) increased the measured backscatter at oblique incidence and decreased it at normal incidence. Additional dry snow did not change the backscatter significantly. These results were attributed to increased ice surface roughness caused by the snow layer and an increase in the dielectric contrast caused by brine wicking from the ice into the snow layer. Consequently, although addition of a snow cover altered the backscatter, it was a thermodynamic effect, resulting from changes in the ice surface when the snow was added. A further increase in the backscatter at all angles was found when the snow was flooded. This enhanced scattering was caused by an increase in the dielectric contrast between the slushy snow and the air.

Modeling studies have shown that the primary factors affecting scattering in the visible and NIR portion of the spectrum are the density, grain size, and wetness of the snow

cover [12]. Microwave modeling shows that both passive and active microwave interactions are also sensitive to changes in grain size and wetness, but only to a lesser extent in density. In the case of emissivity, the addition of snow over a saline ice surface indicates that the snow can impact directly through scattering and absorption mechanisms. In fact, significant signature variations were recorded only after the salinity structure of the snow–ice interface had been modified and metamorphism of the snow grains had taken place—both growth of kinetic forms and rounding and enlarging of the grains.

Evidence from both observational and modeling studies indicate that snow on sea ice plays a central role in the interaction of visible, NIR, thermal infrared (TIR), and microwave energy at the surface and within the volume. The physical mechanisms controlling these interactions indicate that the spectral and temporal evolution of scattering across a variety of frequencies may evolve from a common set of geophysical and thermodynamic characteristics of snow-covered sea ice.

B. Objectives

The primary objective of this paper is to investigate the geophysical and thermodynamic effects of snow in defining the EM interaction within the microwave portion of the spectrum over snow-covered first-year sea ice. We propose to structure this objective by addressing the following two questions.

- 1) If we hold the thermodynamic effects constant, what are the role of physical and electrical properties of snow on microwave scattering and emission? (Geophysical effects.)
- 2) What are the primary thermodynamic properties that influence microwave scattering and emission, and what frequency dependencies exist for these interrelationships? (Thermodynamic effects.)

In what follows, we present the methods that are pertinent to this research. We then present our results as they pertain to the geophysical and thermodynamic effects of snow on scattering and emission. We examine three case studies: Case 1 (cold snow), Case 2 (warm snow), and Case 3 (wet snow). We examine the direct effects of snow and sea ice physical properties on microwave scattering and emission using only Case 1. We then evaluate our data across the three cases to examine the thermodynamic effects on scattering and emission, as determined by the temporal evolution of the system. We then conclude on the salient results of this work, within the limits of this case study, and make recommendations on how this work can be extended within broader scientific and operational contexts.

II. METHODS

Data for this study were collected during January of CRRELEX'94. A large outdoor pond, designated the Geophysical Research Facility (GRF) was used to grow sea ice for this and other experiments conducted during the period 1993–1995. The pond is approximately 18×7.5 m in dimension with a mean depth of 2 m. A unique feature of the pond is the retractable insulated roof fitted with cooling ducts connected

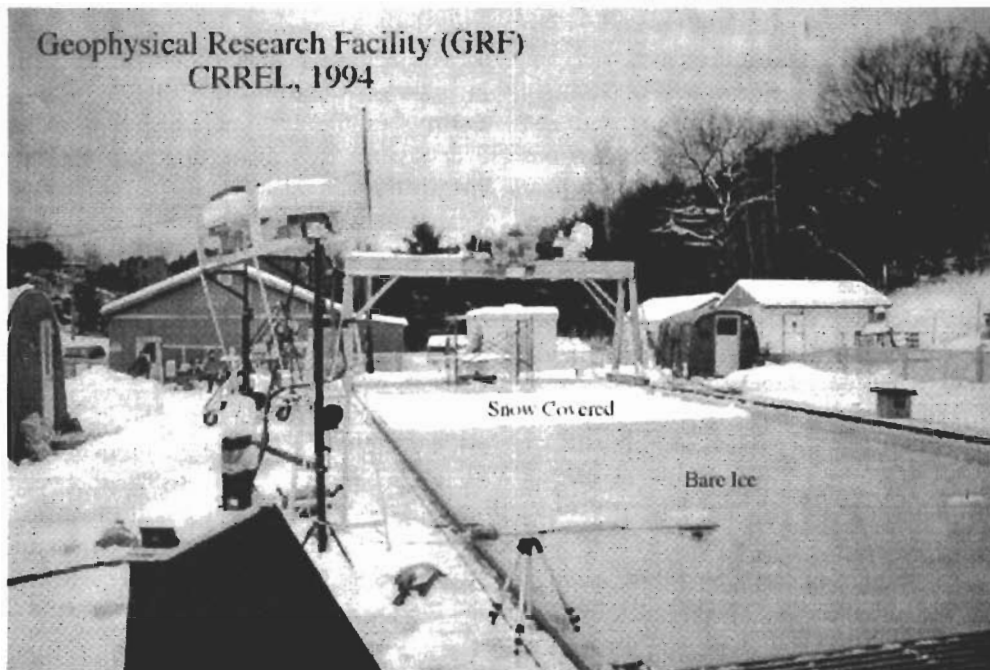


Fig. 1. Photo of the GRF from the CRRELEX'94 experiment. Snow and bare ice surfaces are denoted.

to a refrigeration unit that allows for "under the roof" freezing of sea water in the pond. The pond contained water raised to a salinity of 30 ppt by the addition of a sea salt mixture that closely approximated the composition of Arctic seawater. The ice sheet grown in this experiment was developed entirely under the roof. Freezing was initiated in mid-December 1993 and yielded an ice sheet averaging 29 cm thick prior to beginning the snow experiment. A suite of EM instruments was mounted around the perimeter of the pond and on a gantry that could track along the long axis of the pond (Fig. 1). EM measurements were coupled in space and time with a complete suite of physical and electrical measurements of the snow and sea ice as part of the framework for the overall ONR ARI (see details elsewhere in this issue).

To investigate the role of snow in EM scattering, we selected three cases that span the conditions from winter to advanced melt within naturally occurring snow over sea ice. The cases are limited to this range due to the complexities in the analysis and the logistical constraints of the GRF. The cases were selected during the period January 9–15, 1994, according to the following air temperatures (Fig. 2): Case 1 ($T^{\circ} < -10^{\circ}\text{C}$); Case 2 ($-6^{\circ}\text{C} \geq T^{\circ} \leq -4^{\circ}\text{C}$); and Case 3 ($-3^{\circ}\text{C} \geq T^{\circ} \leq +1^{\circ}\text{C}$).

A. Physical Sampling

The snow physical properties were measured several times per day as a means of determining both the state and thermodynamic evolution of the snow cover on the thin, first-year sea ice surface grown in the GRF. The snow volume and ice surface samples were obtained from snow pits excavated at the south end of the CRREL pond (Fig. 1). Sampling at the pits was done without replacement at a vertical resolution that varied between 2.0 and 0.5 cm, depending on the variable being measured. Snow salinity was measured using a refractometer, and

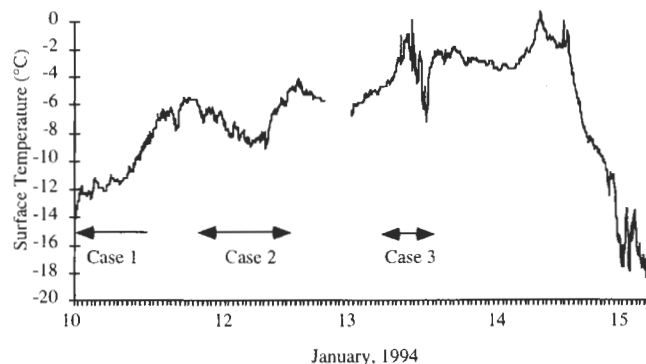


Fig. 2. Surface temperature over the CRRELEX period as measured with a pair of pyrogeometers. Cases 1–3 time frames are denoted.

snow density was measured using the gravimetric approach. Water in liquid phase was measured using a capacitance plate [16]. Snow temperatures were measured at 1-cm vertical spacing extending from the snow–ice interface to the snow surface with 24 AWG, Cu–Co thermocouple junctions. The junctions were embedded in brass tubing (9×0.5 cm), which in turn were fastened at predetermined levels to a wooden dowel. The sensor array (including leads) were painted white to minimize thermal contamination. The snow was backfilled evenly, and the sensor leads were buried to further minimize thermal contamination. Temperatures were logged as 5-min averages to a Campbell Scientific 21X datalogger. Snow grain photographs were obtained at 1-cm intervals through the vertical profile. Samples were removed with a purpose built grid and photographed at a fixed distance using a 35-mm camera and 60-mm micro lens. These photographs were then digitized into a microcomputer, where an operator identified individual grains. Image processing was done to obtain statistical estimates of snow grain area, perimeter

length, and the major and minor axis of the best-fit ellipse for all grains within a particular photo. Since the photographs are a two-dimensional (2-D) projection of the individual snow grains, each estimate is considered a surrogate of the three-dimensional (3-D) counterpart.

B. Modeling Complex Permittivity

The dielectric constant of snow was modeled using the fractional volumes of air, ice, and brine. The volumes were computed based on the observed density, salinity, and temperature of the snow and sea ice. The dielectric constant was modeled using various forms of the Debye equations, depending on the nature of the partial fractions of ice, air, brine, and water in liquid phase. When brine was present in the snow cover, a mixture model was used that considered brine as the “inclusion dielectric” within a dry snow “host dielectric.” When water in liquid phase was present, the model considered the water as the “inclusion dielectric” in a dry snow “host dielectric.” Brine-free saline snow was treated as an ice inclusion within an air “host dielectric.” Further details of these models are available in [13].

C. Electromagnetic Sampling

Microwave emissivities were measured using five radiometers operating at frequencies of 6.7, 10, 18.7, 37, and 90 GHz, respectively. Instrument bandwidths were 300 MHz for 6.7–37 GHz and 1 GHz at 90 GHz. Measurements were made at vertical (VV) and horizontal (HH) polarization by rotating the instruments about their principal axes. Two point calibrations were performed on site. High temperature points were obtained using eccosorb targets whose temperature was carefully monitored, and low temperature points were obtained using the “tipping method.” The spot sizes for the emissivity measurements was on the order of 1-m diameter (transverse) and 1–3 m (1.55 m at 50°) in the vertical plane, defined by the angular scanning. The resulting accuracy in the determination of emissivity is approximately 0.01. Further details on the radiometers and the sampling procedures are described in detail in [6].

The Jet Propulsion Laboratory (JPL), California Institute of Technology, Pasadena, C-band polarimetric scatterometer was used to measure polarimetric backscatter of the snow-covered sea ice. The center frequency is 5 GHz with a bandwidth of 1 GHz. The antenna is a dual-polarized diagonal horn with a beamwidth of 12° and a center-frequency gain of 22.6 dBi. The antenna is pointed in both elevation and azimuth with two independent motors. The radio-frequency (RF) components are temperature controlled at 25 °C. During the experiment, calibration measurements were obtained with corner reflectors and a metallic sphere. The uncertainty in backscatter measurements is approximately 1.2 dB. Further details of data acquisition, processing, and calibration can be found in [21].

The Environmental Research Institute of Michigan (ERIM), Ann Arbor, multifrequency polarimetric radar was used to measure the backscatter of bare and snow-covered sea ice. Center frequencies are 5.25, 10, and 38 GHz with bandwidths

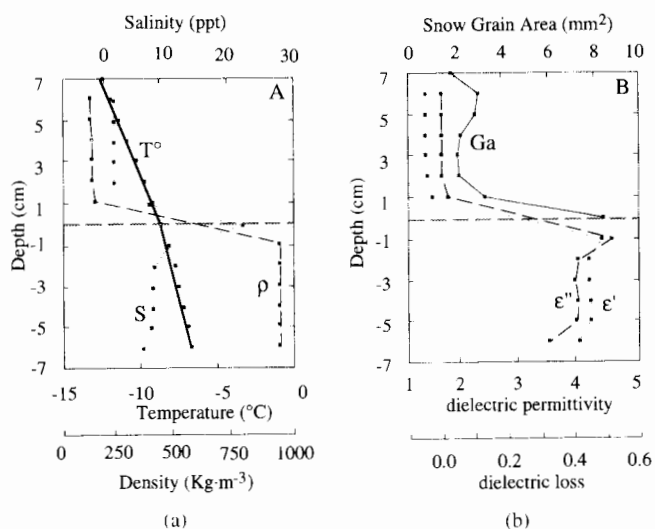


Fig. 3. (a) Temperature, salinity, and density and (b) average snow grain radius, permittivity, and loss for Case 1.

of 1–2 GHz. An array of four standard gain antennas are used for each frequency of operation and allow simultaneous like- and cross-polarization reception. Use of separate antennas for transmission and reception provides much improved separability between antenna-to-antenna leakage from the received signal and the ability to measure smaller radar cross-sections. Antenna two-way beamwidths range from 16 to 6°, depending on frequency and polarization. The antenna array was positioned in elevation electromechanically with angles from nadir to the sky. Sky returns were used to document the system noise floor and the minimum measurable cross section. Along and across positioning control about the ice tank was facilitated by moving the GRF gantry in the along-track direction or the antenna cluster about the gantry in the across-track direction. Short-term calibration is facilitated by monitoring the antenna-to-antenna leakage signal. Absolute calibration was made by using a pair of small- and moderate-sized corner reflectors and a dihedral corner reflector at 0, 22.5, 45, 67.5, and 90° orientation angle. The uncertainty in backscatter measurements is typically 2 dB due to the limited number of independent spatial samples that may be obtained.

Infrared observations were obtained using a Heimann KT-19 infrared radiometer. It records TIR radiation in the 8–14- μ m band to a precision of 0.1 K and an absolute accuracy of about 0.3 K. Calibrations were performed before and after the experiment using a precision infrared blackbody constructed at the Applied Physics Laboratory, University of Washington, Seattle.

D. Forward Scattering and Emission Modeling

A combined surface–volume scattering model based on the radiative transfer formulation [14] for an inhomogeneous layer above an inhomogeneous half space is developed using a dense medium phase function. This phase function reduces to the standard phase function for sparse media when scatterers are more than a wavelength apart and volume fraction is small. It includes coherent scattering from a group of randomly positioned scatterers within a unit volume when the medium is dense [15]. Its effect is to decrease the effective number

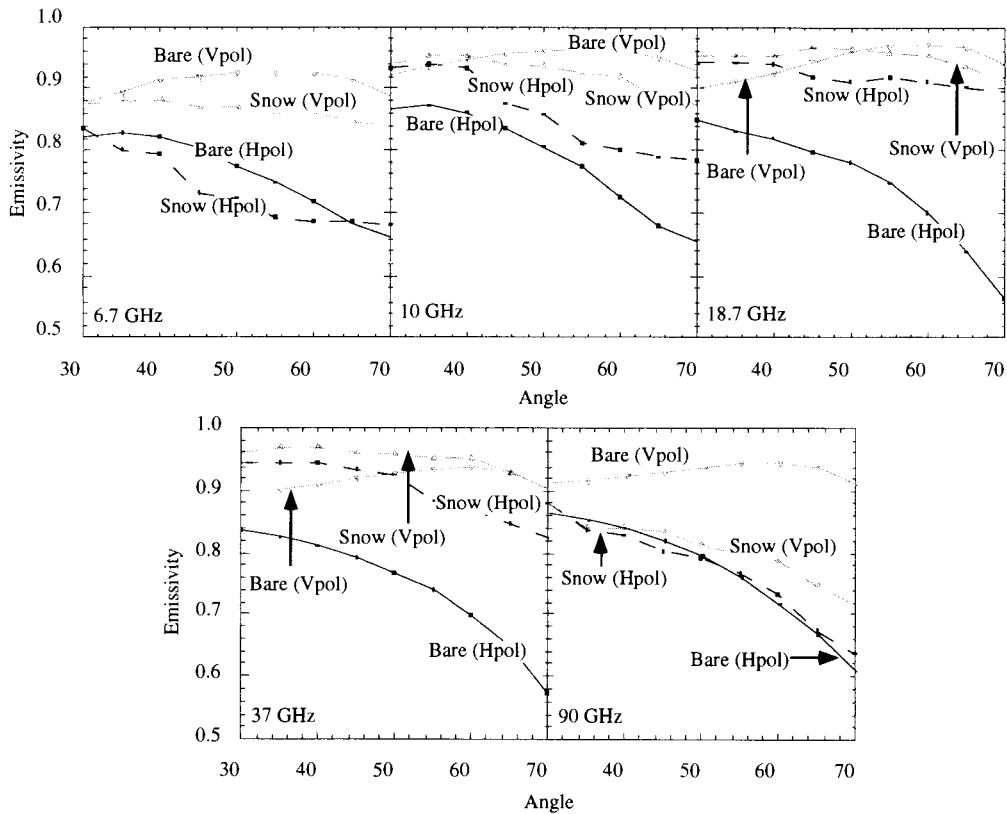


Fig. 4. Passive microwave observations of Case 1 for snow-covered and snow-free cases at 6.7, 10, 18.7, 37, and 90 GHz.

density of the scatterers and hence the scattering albedo of a discrete inhomogeneous medium relative to that of a sparse medium. The phenomenon of group scattering is a function of frequency, volume fraction, and the size of the scatterer. Generally speaking, for snow, it takes place when the operating frequency is high (over 18 GHz) and/or the volume fraction is large (around 0.2–0.3).

In microwave emission, a principal unknown is the effect of interface roughness on direct emission. In the literature, an *approximate* formula has been provided for estimating the decrease in emission due to interface roughness between two media. It is of the form $\exp[-k^2 \sigma^2 (\sqrt{\epsilon_2} \cos \theta_1 - \sqrt{\epsilon_1} \cos \theta_2)^2]$, where $\sqrt{\epsilon_1}$, $\sqrt{\epsilon_2}$ represent the real parts of the square root of the relative permittivities in medium 1 and 2, k is the wavenumber in air, σ is the rms height of the interface roughness, and θ_1 , θ_2 are the directional angles in crossing the interface. Since the correct formula is not known, we shall use this formula as a guide and σ is adjusted to fit data. Thus, σ in this formula is not the real rms height of the surface and cannot, in general, be expected to take on a fixed value as we change frequency.

We also modeled microwave emissivity using a wave theory model based on the strong fluctuation theory (SFT) in the bilocal approximation. The formulation presently applied is a multilayer implementation of the theory developed by Stogryn describing semi-infinite plane parallel but vertically inhomogeneous media [16]. A more detailed description is provided in this issue (see [22]). In the present case, a 16-layer model was used to describe the cases of bare ice and the same ice with a snow layer.

In both the radiative transfer and SFT models, we utilized coincident physical observations of the sea ice and snow microstructure for initialization. Thermodynamics were modeled and or measured *in situ*. Direct measurements of emission and scattering were obtained coincident with the physical property sampling and are compared directly with model predictions.

III. RESULTS AND DISCUSSION

In what follows, we present the physical and EM measurements for the three cases observed during the CRRELEX (observations). We then utilize the forward scattering models, described above, to assess model fits to the data and examine both the geophysical and thermodynamic effects of snow on microwave scattering and emission (modeling).

A. Observations

Case 1: The snow cover on the thin first-year sea ice sheet at the GRF was representative of fall conditions over newly formed sea ice in the Canadian Arctic Archipelago. Air temperatures in Case 1 were cold, creating a large temperature gradient within the snow volume and a smaller gradient within the sea ice (Fig. 3). Salinities showed a maximum within the basal layer of the snow volume decreasing upwards into the snow and down into the ice volume (Fig. 3). Brine wicking was responsible for the increased brine volumes in the basal snow layer [17], and desalination processes during ice growth create the decreased salinity within the ice volume. Density within the snow volume was reasonably uniform due to the absence of sintering and saltation processes within the laboratory environment. The average snow grain sizes

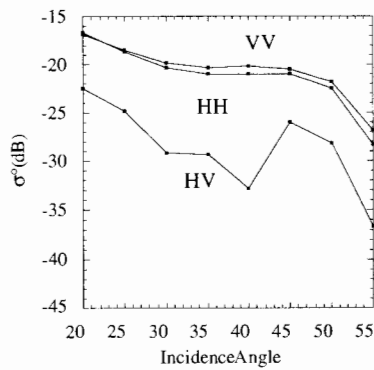


Fig. 5. Active microwave observations (JPL system) of Case 1 for snow-covered and snow-free surfaces at 5.0 GHz. The approximate location of the snow boundary occurs at 45°.

increased toward the basal layer due to the aggregation of grains caused by the presence of large brine volumes. The modeled complex permittivity of the snow and ice showed values typical of low-density cold snow and thin first-year sea ice (Fig. 3). The ice volume was typical of young Arctic sea ice with a small surface frazil layer, columnar subsurface structure, and a surface that is considered smooth at microwave frequencies. The microstructural characteristics of this ice sheet remained essentially unchanged throughout the duration of the experiment. Similarly no significant changes in the salinity profile were observed, except those due to the brine wicking described above.

Direct measurements of the EM scattering and emission fields were obtained from both snow-covered and snow-free ice. Emissivity for bare ice and snow-covered ice showed the typical response for cold, thin first-year ice surfaces (Fig. 4). The effect of the snow cover is evident above about 10 GHz. Grain sizes (Fig. 3) are sufficiently large that scattering can be expected to directly effect microwave emission. Indirectly, we can expect there to be an impedance matching process, whereby the complex permittivity at the snow–ice interface will be different than what is observed over the bare ice surface. This is evident in the divergence of the HH-polarization snow versus bare surfaces as we consider increasing frequencies (Fig. 4). The divergence increases to 37 GHz; then emissivities become equal at 90 GHz due to the frequency dependency of this mechanism.

Observations of the active microwave scattering for Case 1 was constrained by the fact that a large area was needed to collect independent samples. Of the two scatterometer systems used, one was oriented along the long axis of the GRF (Fig. 1), which meant that incidence angles passed from the snow-covered to snow-free portions of the surface (JPL Scatterometer). The other scatterometer (ERIM) was mounted on the moveable gantry over the pond and used to collect incidence angle data within the snow and bare ice surfaces. Results from the JPL system clearly show the effect of volume scattering within the snow layer and the transition to the ice-free surface at nadir angles above about 45° (Fig. 5). The ERIM scatterometer data show little difference in the scattering at like polarization for 5.3 and 10 GHz, but a substantial increase in scattering for the snow versus bare surface at 38 GHz (Fig. 6).

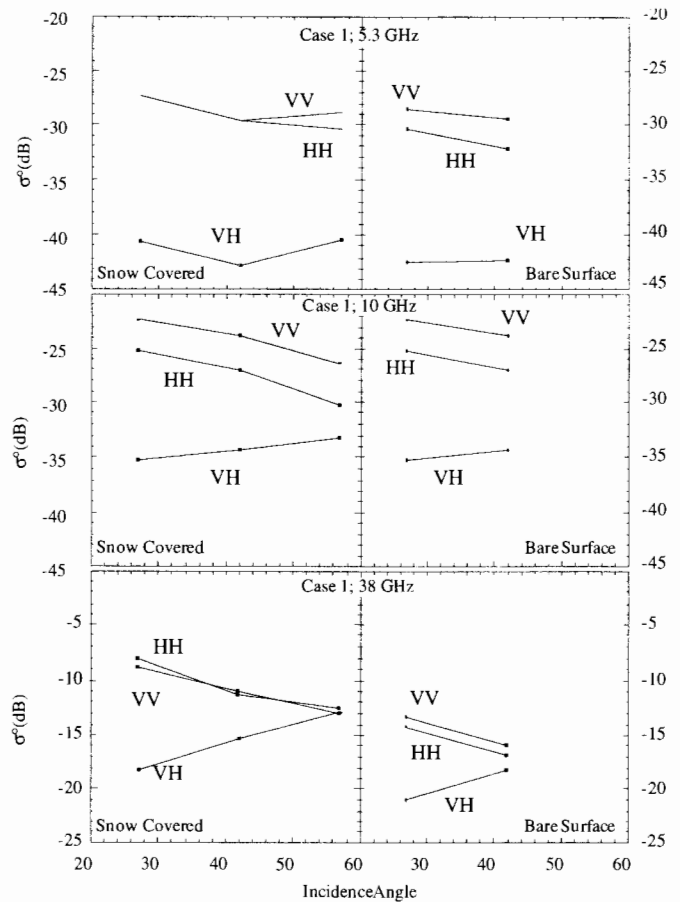


Fig. 6. Active microwave observations (ERIM system) of Case 1 for snow-covered and bare ice surfaces at 5.3, 10, and 38 GHz.

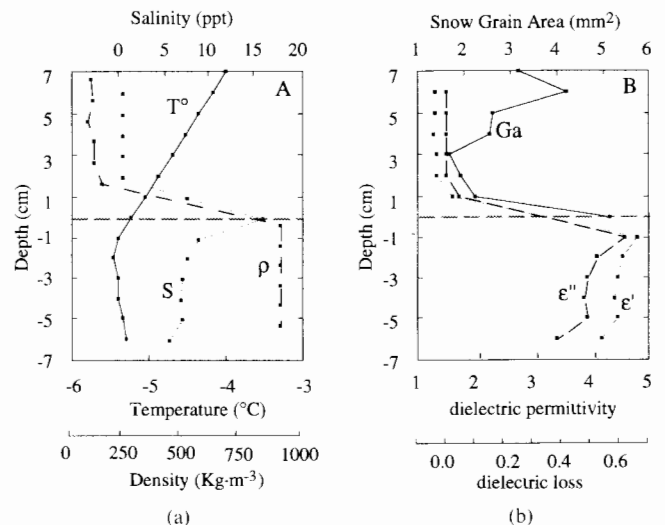


Fig. 7. (a) Temperature, salinity, and density and (b) average snow grain radius, permittivity, and loss for Case 2.

Case 2: Air temperatures in Case 2 warmed, creating a positive temperature gradient within the snow, but due to the low thermal diffusivity of the snow volume the ice temperature remained relatively cool (Fig. 7). Salinities showed a maximum within the basal layer of the snow volume decreasing upward into the snow and downward into the ice volume (Fig. 7). The higher interface temperatures created large brine

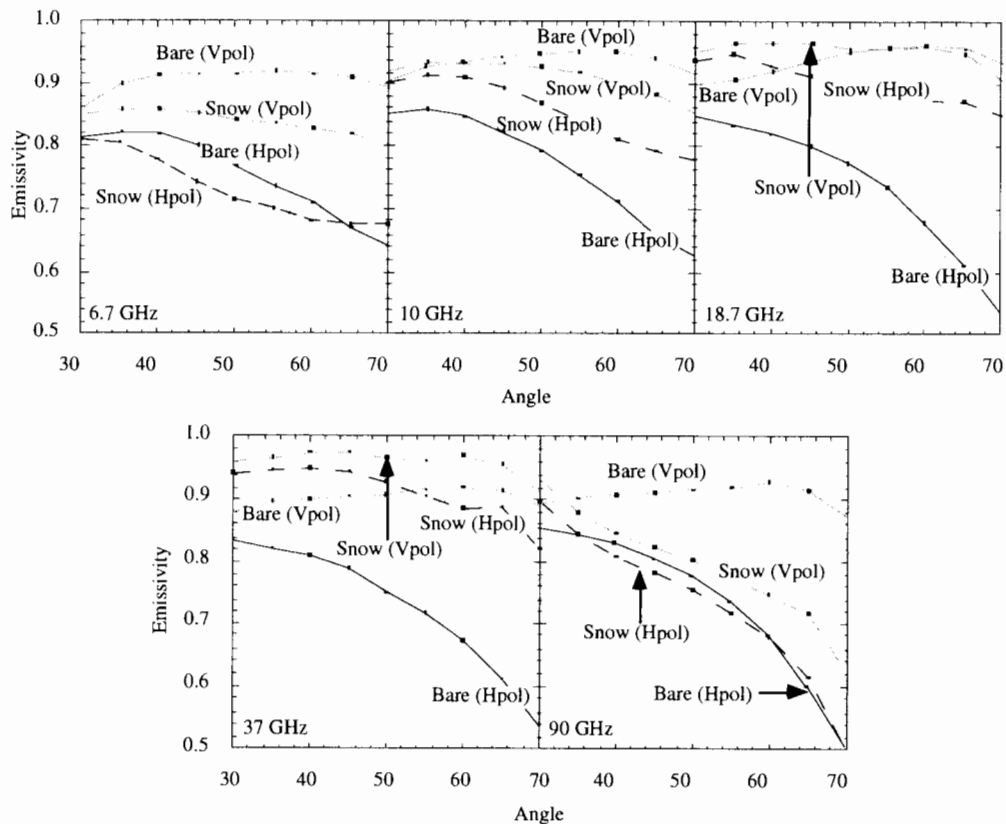


Fig. 8. Passive microwave observations of Case 2 for snow-covered and snow-free cases at 6.7, 10, 18.7, 37, and 90 GHz.

volumes within the basal layer of the snow cover and at the surface of the sea ice. Grain sizes seemed to have decreased between Cases 1 and 2, but we consider this change within the error margins of our sampling method. Large grains occurred near the surface and within the basal layer of the snow volume (Fig. 7). Both the real and imaginary parts of the complex permittivity increased slightly within the ice volume due to the elevated temperature at the interface. This increase was not as large as it might have been because the salinity at the snow-ice interface was lower than in Case 1 (see Figs. 3 and 7).

Direct measurements of the EM scattering and emission were obtained from both snow-covered and snow-free ice. Microwave emission tended to increase in emissivity as a function of wavelength to 37 GHz; then it decreased at 90 GHz (Fig. 8). The separation of bare and snow-covered ice appeared to increase with frequency up to but not including 90 GHz. This is a result of the decreasing reflectivity with increasing frequency within the basal layer of the snow relative to the ice surface, combined with an increase in opacity and degree of volume scattering of the snow layer. In the snow-free case, the surface reflectivity of the ice surface was not masked by the snow. Consequently, the frequency variations are much smaller and the spectra much flatter. The snow layer also decreases the difference between $\epsilon(V\text{-pol})$ and $\epsilon(H\text{-pol})$ by reducing the system reflectivity at H-pol much more strongly than at V-pol (Fig. 8).

Results from the scatterometer observations (JPL system) indicate that the snow boundary on the CRRELEX surface was not nearly as distinct as it was in Case 1 (see Fig. 5

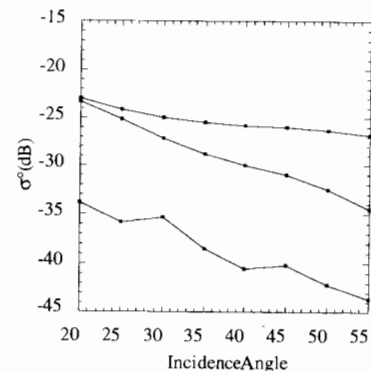


Fig. 9. Active microwave observations (JPL system) of Case 1 for snow-covered and snow-free surfaces at 5.0 GHz. The approximate location of the snow boundary occurs at 45°.

versus Fig. 9). The rate of change in scattering as a function of incidence suggests that the volume-scattering component of the total scattering coefficient was large in Case 2 (Fig. 9). Results from the ERIM system are limited to the snow-covered case only (Fig. 10). Results from this system also suggest that volume scattering was dominant in Case 2. The frequency diversity of these data suggest that increasing scattering from 5.3 to 10 and 38 GHz could be a function of the relative roughness of the ice interface and the effect of grain size on the shorter wavelengths with increasing frequency.

Case 3: Air temperatures in Case 3 was such that phase transitions began to occur within the surface layer of the snow volume. This process lead to equitemperature metamorphosis within the snow volume. Density increased within the snow

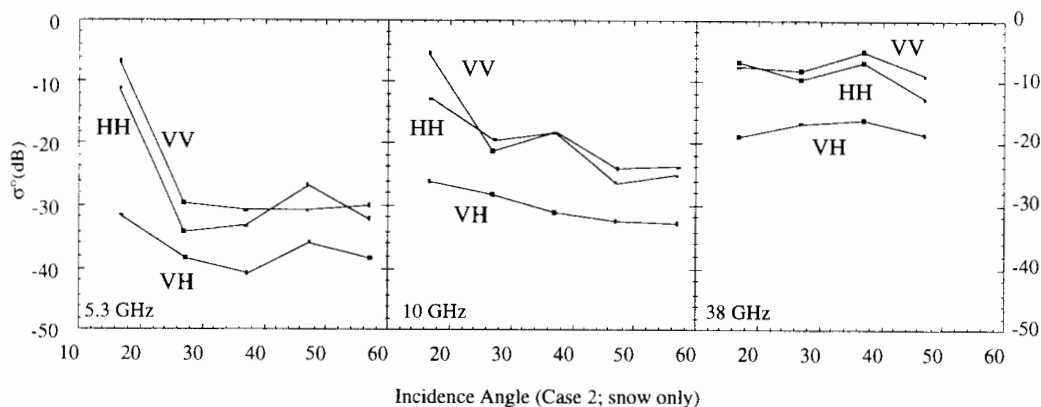


Fig. 10. Active microwave observations (ERIM system) of Case 2 for the snow-covered surface only at 5.3, 10, and 38 GHz.

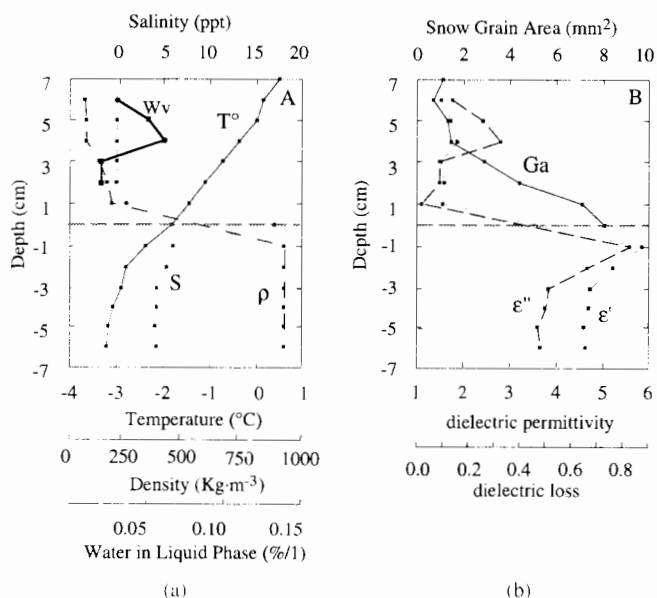


Fig. 11. (a) Temperature, salinity, and density and wetness and (b) average snow grain radius, permittivity, and loss for Case 3.

volume, particularly in the lower 3 cm. There was a slight increase in grain size (relative to Case 2) although this change is within our measurement uncertainty. We observed significant amounts of water in liquid phase within the snow volume (Fig. 11). There was a slight density horizon within the snow volume at about 4 cm (up from the ice surface). We observed a maximum in the water volume at this level (Fig. 11). This increased density and water in liquid phase created a larger permittivity and loss at this layer (relative to Case 2). The presence of water in liquid phase in the basal layer of the snow and the elevated brine volumes in these layers resulted in substantially higher permittivities and losses in both the basal layer and at the first-year ice surface (relative to Cases 1 and 2).

Direct measurements of the EM fields were limited to passive microwave emission for this particular case. Results illustrate the dramatic effect of water in liquid phase on the emissivity at each of the frequencies measured (Fig. 12). We note that even at 6.7 GHz there is a large separation in the V- and H-polarizations for both bare and snow-covered surfaces. The minimum separation now occurs between 18- and 37-GHz

frequencies, allowing 90 GHz more separation than either of Case 1 or 2. We would expect emission from the ice and from the water in liquid phase within the snow to both contribute to the measured emissivity. Grain sizes are also expected to affect the measurement of emissivity through the volume scattering at these frequencies.

B. Modeling

1) *Geophysical Effects:* By using forward scattering and emission models we are able to evaluate our ability to 1) successfully model the observed EM fields and 2) evaluate the relative roles of various geophysical variables on the scattering from the snow cover. These effects are evaluated for Case 1 only.

In modeling the emission from snow-covered sea ice, we selected the radii of scatterers in snow and ice media to be 0.06 and 0.018 cm and their volume fractions as 0.2 and 0.05, respectively. These model parameters remain the same for all cases considered in this section for both passive and active sensing and for interpreting bare and snow-covered saline ice.

The radiative transfer model predictions were excellent at each of the frequencies and polarizations. Our results show that up to 18.7 GHz, emission is predominantly accounted for by direct emission. The contribution by volume scattering is appreciable only at 37 GHz. The presence of snow substantially raises the overall level and alters the angular shape, especially of horizontally polarized emission. With snow cover, the Brewster angle effect is not significant (Fig. 13) and there is a gradual rise in emission from 10 to 37 GHz. We speculate that the decrease in permittivity with frequency plus the aggregate scattering effect overcome the rate of increase in single-scattering albedo over this frequency range (Fig. 13).

In Fig. 14, we show comparisons between radiative transfer model predictions and data for microwave scattering by bare and snow-covered saline ice. The volume-scattering parameters for ice are fixed as described earlier and surface roughness parameters are selected to fit the data at 5.3 GHz. Once the roughness parameters are determined, they remain unchanged at 10 and 38 GHz. The correlation function for the interface roughness is taken to be exponential. At the air-snow interface, rms height and correlation length are 0.07 and 0.4 cm; at the snow-ice interface, they are 0.07 and 0.37 cm for all frequen-

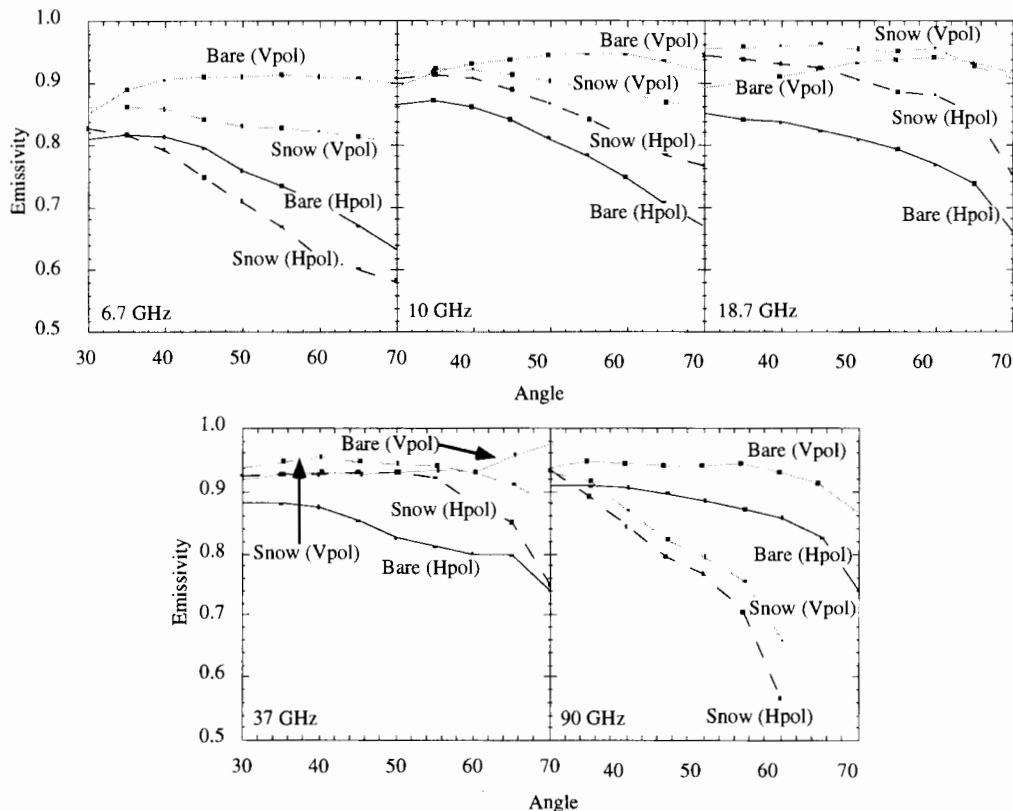


Fig. 12. Passive microwave observations of Case 3 for snow-covered and snow-free cases at 6.7, 10, 18.7, 37, and 90 GHz.

cies. Here again, agreement is obtained between model trials and observed data. Results indicate that at 5.3-GHz, volume scattering is important. It is lower than surface scattering when there is no snow and becomes higher than surface scattering when there is snow. At 10 GHz, surface scattering exceeds volume scattering by a large margin but volume scattering is still appreciable, especially when there is snow cover. This is also true for bare ice at 38 GHz. However, with snow cover, volume scattering at 38 GHz from snow is the dominant factor. This is because the snow layer acts as an attenuator to surface scattering from the snow-ice interface. The spacing between vertical and horizontal polarizations narrows, when there is snow cover. This narrowing also increases with frequency for both bare and snow-covered saline ice. This is because the surface acts rougher and volume scattering is stronger at high frequencies.

We also modeled the geophysical conditions observed in Case 1 with the SFT (Fig. 15). Results from these model trials are presented in terms of emissivity and scattering as a function of frequency at a 50° nadir angle (Fig. 15). The set of physical parameters for the snow and ice, described above (Fig. 3), are used, except that the salinity profile near the bottom of the ice is adjusted to correct for brine drainage during core extraction and sampling. The model results in both cases represent an average over a range of slight perturbations in the salinity profile to smooth out fringe effects that arise from coherent wave interactions for a particular structural realization. Although the SFT formulation is quite different than the radiative transfer model and does not include surface scattering, the agreement between observations and modeled

results is quite good, particularly at 10 and 37 GHz. For bare ice, the SFT model results are slightly higher than the observations, particularly at vertical polarization, and the difference is slightly greater for higher frequencies. This suggests that the introduction of surface scattering would improve the agreement. In the case of backscattering, the SFT model results lie 5–10 dB below the observations, depending on frequency. For bare ice, the SFT model results deviate more strongly for increasing frequency (Fig. 15). For snow-covered ice, the curves are approximately equidistant. These results confirm that a surface-scattering model may be required. Comparison of the radiative transfer and SFT models illustrate that when volume scattering dominates, SFT and radiative transfer produce comparable results. The lack of explicit surface-scattering mechanisms in SFT limits its utility under geophysical and thermodynamic conditions when a significant surface-scattering term is present.

We can also use the radiative transfer model to examine the relative contributions of various geophysical parameters on EM interaction. The role of grain size is illustrated for both emission and scattering (Fig. 16). In Fig. 16, the solid line represents total emission and the dash line represents direct emission, excluding volume-scattering terms. Clearly, emissivity is dominated by direct emission from saline ice through the snow layer. Hence, the influence of grain size is small but the trend is clearly a drop in total emission as the grain size increases. This is due to an increase in scattering by the snow layer. This fact is confirmed where backscattering is seen to increase dramatically with increasing grain size (Fig. 16). This impact of grain size in microwave scattering is

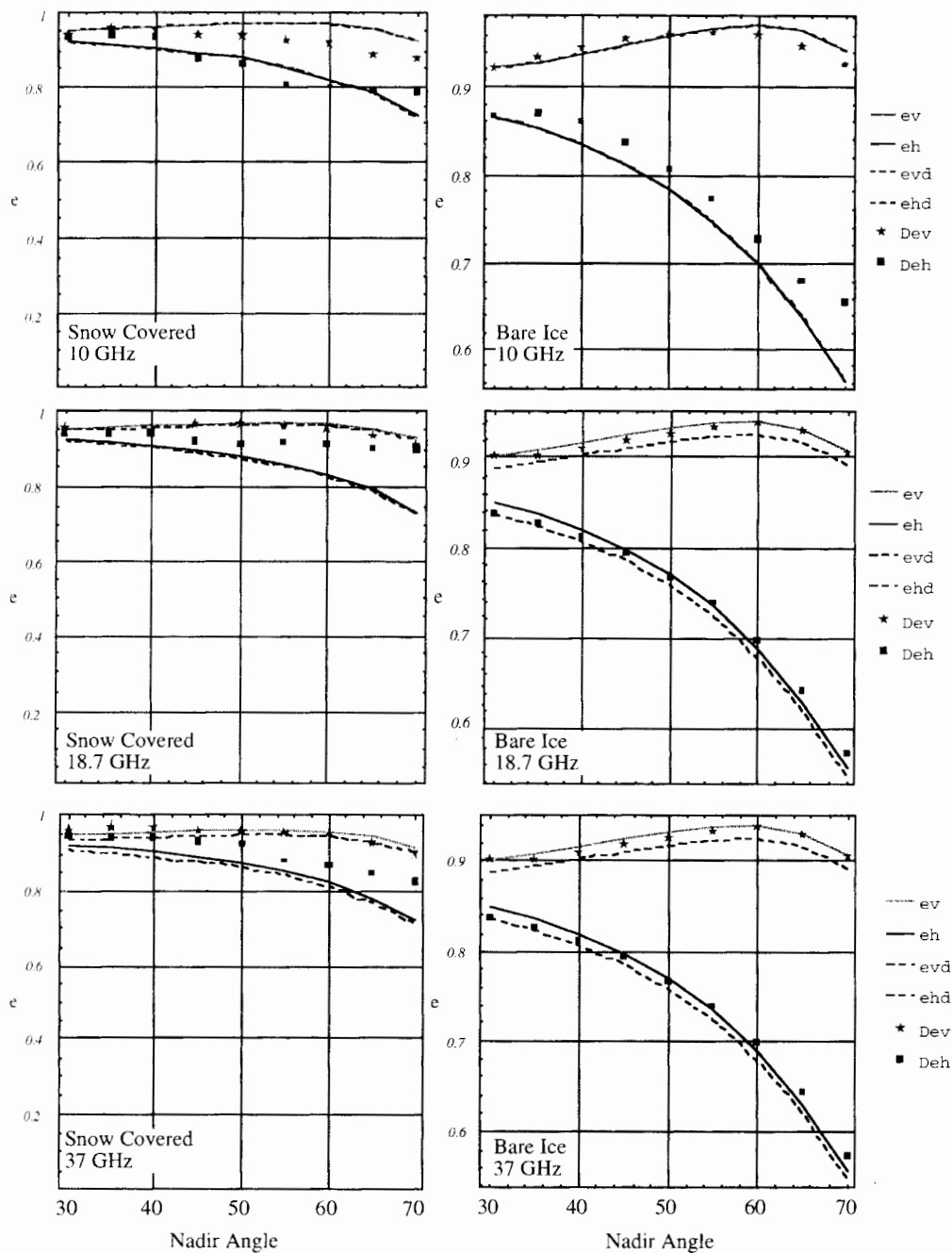


Fig. 13. Observed (Dev and Deh) versus modeled (radiative transfer) emissivity as a function of angle for 10-, 18.7-, and 37-GHz frequencies for H- and V-polarization. Bare and snow-covered cases are denoted. Note that e_v and e_h are the total emissivity for V- and H-polarizations and e_{vd} and e_{hd} are the emissivities minus volume-scattering effects.

due partially to our selection of 40° incidence, where volume scattering by snow becomes the major contributor after the grain radius exceeds 0.13 cm. In Fig. 16, V_{vv} , V_{hh} denote volume scattering, S_{vv} , S_{hh} denote surface scattering, and VV, HH denote total backscattering in vertical and horizontal polarizations.

The role of the volume fraction of snow on emission and scattering is shown in Fig. 17. For a sparse medium theory [14], in which inhomogeneities are assumed to scatter independently, albedo and the extinction coefficient will increase with volume fraction, provided that absorption remains constant. Hence, we expect emission to decrease continuously as volume

fraction increases. We find, however, that as volume fraction increases, the inhomogeneities can no longer scatter independently because there may be more than one scatterer within the distance of a wavelength. Thus, these inhomogeneities tend to scatter as a group in some coherent manner. As a result, the scattering albedo decreases, causing an increase in emission. In Fig. 17, this change takes place around a volume fraction of about 0.16 at 18.7 GHz. In the case of microwave scattering, the same type of change takes place at a volume fraction of 0.35 because the operating frequency is 10 GHz. Note that the portion of backscattering due to air-snow and snow-ice interfaces is not affected by volume

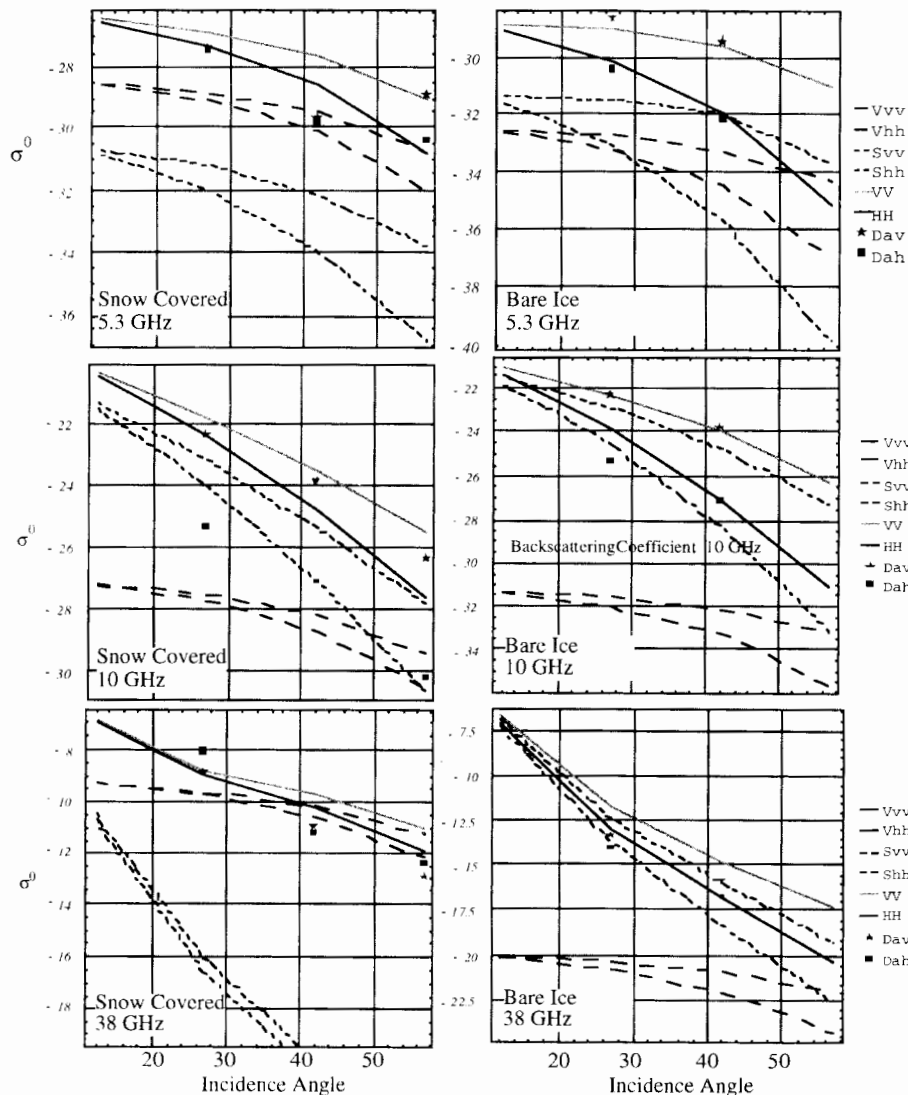


Fig. 14. Observed versus modeled (radiative transfer) scattering as a function of angle for 5.3, 10, and 38 GHz (ERIM system) for VV- and HH-polarizations. Bare and snow-covered cases are denoted.

fraction changes. Hence, surface-scattering curves appear as constants in Fig. 17. Results from the SFT modeling confirm these relationships, indicating that the snow volume fraction affects both scattering and emission as a function of the number density of scatters available within the snow cover.

2) *Thermodynamic Effects:* Although there appears to be numerous geophysical effects of snow on scattering, recent evidence shows that thermodynamic effects (on microwave scattering and emission) are also observable from satellite and aerial remote-sensing data [9], [18]–[20]. The effects examined here are all related to the thermodynamic controls on the geophysical and electrical properties of the snow and sea ice. By examining the temporal evolution across Cases 1–3, we can examine the specifics of scattering and emission from a cold snow cover (Case 1) through a warming trend (Case 2) to the presence of water in liquid phase within the snow cover (Case 3). To constrain our discussion, we limit the amount of data presented here to the change in emissivity between Cases 1 and 2 and Cases 1 versus 3 for 18.7 and 90 GHz. Results

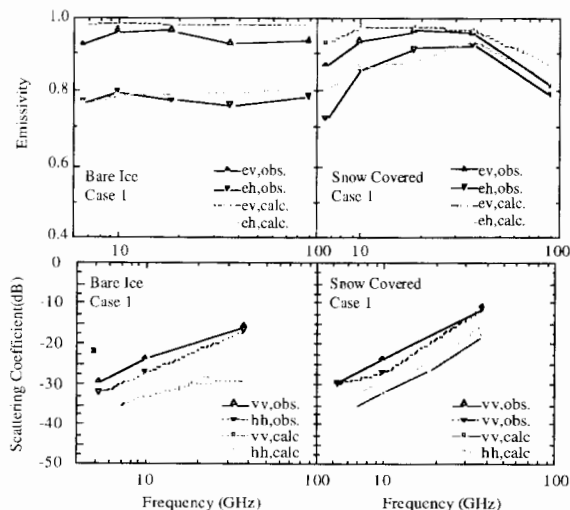


Fig. 15. Comparison of observed and SFT model values of emissivity and the scattering coefficient versus frequency at a nadir angle of 50° for bare and snow-covered sea ice (Case 1).

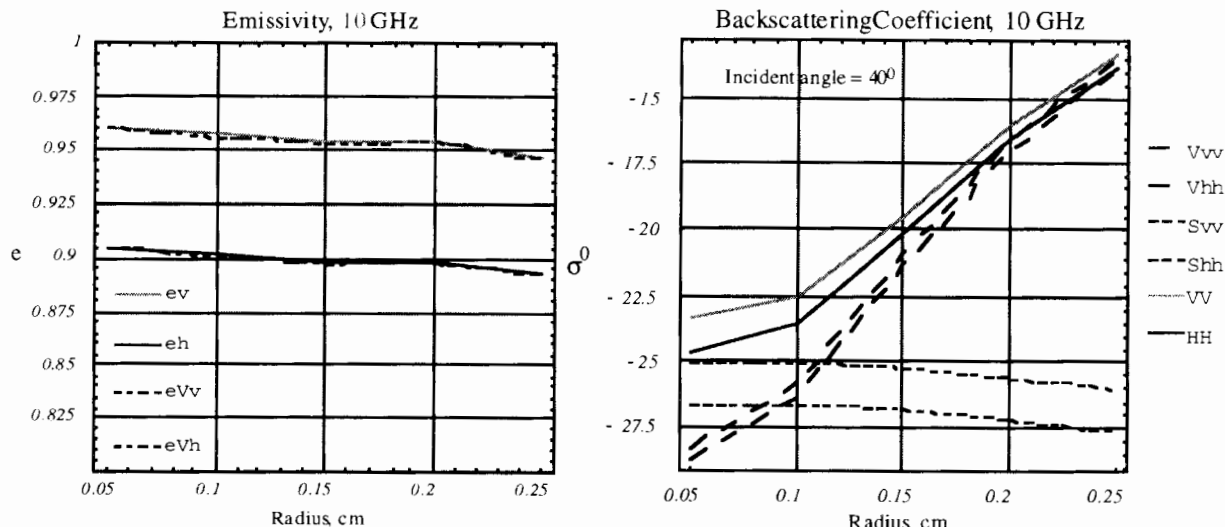


Fig. 16. Effect of grain size on microwave emissivity and scattering at 10 GHz using the radiative transfer model.

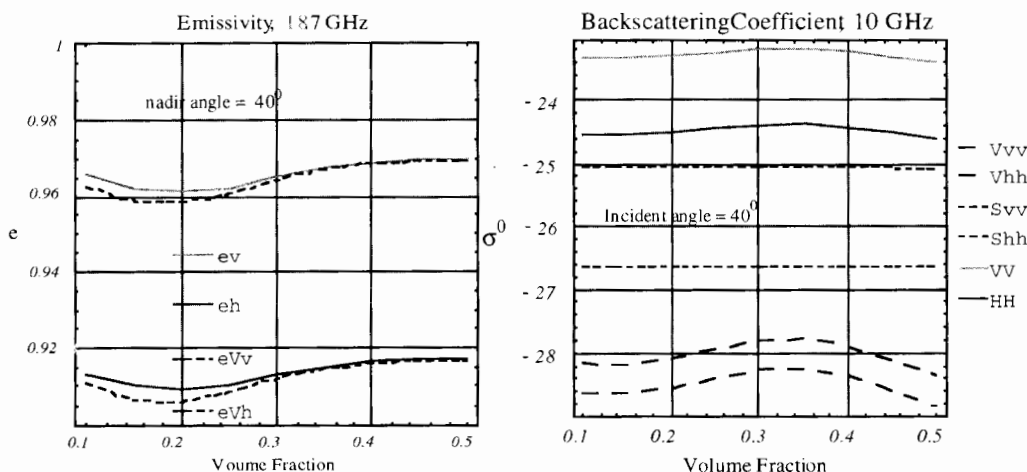


Fig. 17. Effect of snow volume fraction on microwave emissivity and scattering at 18.7 and 10 GHz using the radiative transfer model.

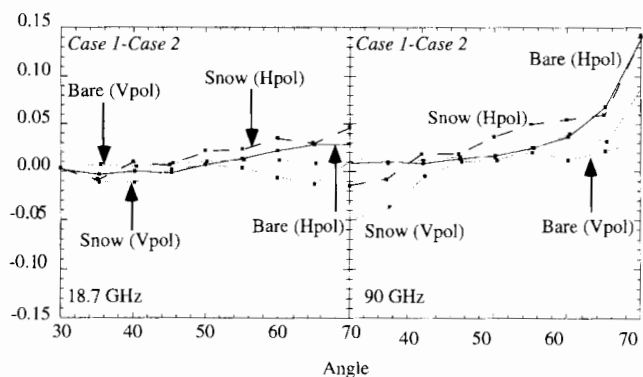


Fig. 18. Change in microwave emissivity between Case 1 (cold) and Case 2 (warm) at 18.7 and 90 GHz.

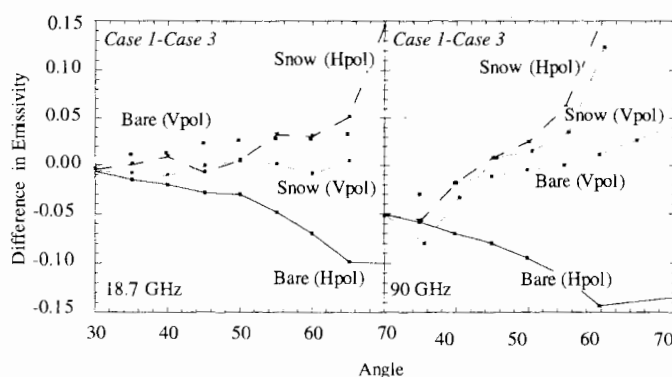


Fig. 19. Change in microwave emissivity between Case 1 (cold) and Case 3 (wet) at 18.7 and 90 GHz.

show that only a small change occurred between the cold and warm cases at the lower frequency (Fig. 18), but as expected the change in emissivity was larger at the higher (90 GHz) frequency. This results from the fact that the dielectric constant is frequency dependent and changes only slightly at 18.7 GHz but changes more dramatically at 90 GHz. The tendency for higher differences in emissivity at higher incidence angles illustrates the role of volume dielectrics and scattering in

the case of microwave emission. As the interaction volume increases (through a steeper nadir angle), the effects of grain scattering and impedance matching between the snow basal layer and ice surface are enhanced (Fig. 18).

The thermodynamic processes creating the changes in Fig. 18 are enhanced when we compare Case 1 with Case 3 (Fig. 19). This is due to the strong influence water in liquid phase has on the dielectric constant of the snow and the

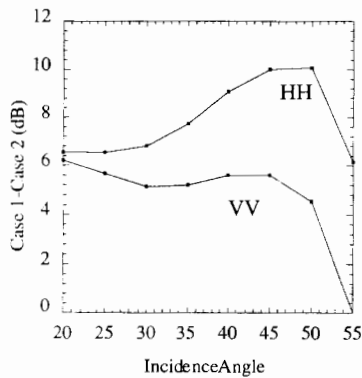


Fig. 20. Change in microwave scattering at 5.0 GHz at VV- and HH-polarization. Data are from the JPL scatterometer. The snow-bare ice boundary is at approximately 45° incidence.

role of elevated brine volumes at the surface of the first-year sea ice. Results show a general increase in the difference in emissivity (Case 3 has a smaller emissivity than Case 1), except for the case of the bare surface at H-polarization. The increase in the differences are due to the enhanced volume scattering in the near-surface layers at 90 versus 18.7 GHz. This causes a decrease in the surface emissivity at these frequencies. We speculate that the bare ice surface (H_{pot}) shows a decrease in the difference in emissivity due to the desalination of the ice surface (caused by the elevated temperatures). This desalination gives rise to a degree of small-scale porosity that tends to decrease selectively the reflectivity at the higher frequencies. Although not depicted here, the 6.7-, 10-, and 37-GHz frequencies showed results consistent with this interpretation.

Although limited to the temporal sequence, represented by Cases 1 and 2, microwave scattering also appears to be affected by the warming of the snow volume. Results show (Fig. 20) that the change in the relative scattering coefficient (σ°) was considerable between Cases 1 and 2 (JPL scatterometer). The decrease in scattering (increase in difference) was largest at the higher incidence angles (40–50°). The large difference between HH- and VV-polarizations suggests that the decrease in scattering, particularly at HH-polarization, was due to a reduction in the volume-scattering term in defining the total σ° . The reduction in scattering in Case 2 is likely due to the increase in the imaginary part of the complex permittivity between the two cases, combined with the fact that the snow grains were sufficiently small that they contributed little to the volume scattering from the basal layer of the snow volume.

IV. CONCLUSIONS

The objectives of this paper were to examine the geophysical and thermodynamic controls on microwave scattering and emission from the perspective of snow on sea ice. In particular, we have focused on defining the geophysical (grain size, density, salinity, etc.) and thermodynamic (temperature magnitude and change) controls on the EM interaction within the semicontrolled laboratory conditions of the GRF.

Results of the geophysical effects indicate that snow begins to have an effect on emission above about 37 GHz and above 5 GHz for active microwave scattering. We understand

these effects to be driven by grain size and its contribution to volume scattering in both passive and active interactions within the volume. The presence of snow substantially raises the overall level and alters the angular shape, especially of horizontally polarized emission. With snow cover, the Brewster angle effect is not significant and there is a gradual rise in emission from 10 to 37 GHz. We find emissivity to be dominated by direct emission from saline ice through the snow layer. Hence, the influence of grain size is small but the trend is clearly a drop in total emission as the grain size increases. This fact is confirmed as backscattering is seen to increase dramatically with increasing grain size (Fig. 16). Results indicate that at 5 GHz, volume scattering is important. It is lower than surface scattering when there is no snow and becomes higher than surface scattering when there is snow. At 10 GHz, surface scattering exceeds volume scattering by a large margin but volume scattering is still appreciable, especially when there is a snow cover. The spacing between vertical and horizontal polarizations narrows when there is snow cover. This narrowing also increases with frequency for both bare and snow-covered saline ice. This is because the surface acts rougher and volume scattering is stronger at higher frequencies. We find that the role of the volume fraction of snow on emission and scattering is a complex relationship between the number density of scatterers relative to the coherence of this scattering ensemble. At low volume fractions, we find that independent scattering dominates, resulting in an increase in albedo and the extinction coefficient of the snow. As the volume fraction increases, we speculate that the inhomogeneities no longer scatter independently but rather in a coherent fashion. This results in a decrease in the scattering albedo and a corresponding increase in emission. We find that this change takes place at volume fractions above 0.16 at 18.7 GHz. In the case of microwave scattering, the same type of change takes place at a volume fraction of 0.35 when the operating frequency is 10 GHz (Fig. 17).

Snow also effects microwave scattering and emission through the role that thermal diffusivity and conductivity play in the definition of snow grain metamorphism, vertical brine volumes, and the distribution of water phase within the snow/ice system. Prior to the presence of water in liquid phase within the snow volume, we find that the thermodynamic effects are dominated by an impedance matching processes across the snow-ice interface. We find that the complex permittivity at the snow-ice interface is considerably higher than over the bare ice surface. This is because the snow layer produces a warmer interface than exists coincidentally over the bare ice surface. This warmer interface increases the brine volume in the basal layer of the snow, thereby creating a "dielectrically rough" interface. This phenomena leads to the notion that for a constant ice thickness, surface rms and correlation length, and salinity, the complex permittivity of the snow-ice interface will be driven by the thickness of the snow volume. This phenomenon is being exploited as a means of estimating snow thickness distributions from the time-series scattering over snow-covered first-year sea ice [9], [20].

More specifically, our results show that only a small change occurred between the cold and warm cases at the lower frequency (Fig. 18), but as expected the change in emissivity

was larger at the higher (90 GHz) frequency. We attribute this change to the fact that the dielectric constant is frequency dependent and changes only slightly at 18.7 GHz relative to 90 GHz. The tendency for higher differences in emissivity at higher incidence angles illustrates the role of volume dielectrics and scattering in the case of microwave emission. Once water in liquid phase appears within the snow cover, we find that both emission and scattering are directly effected by the high complex permittivity of this volume fraction within the snow layer.

It is becoming increasingly apparent that snow plays a important role in the exchange of mass and energy across the ocean-sea, ice-atmosphere interface. Snow regulates the equilibrium thickness of the sea ice because of its lower thermal conductivity, yet the amount and distribution of snow on sea ice cannot be currently measured remotely, accurately modeled, or otherwise estimated. This severely increases our uncertainty regarding the physical response of the ocean-sea, ice-atmosphere interface to projected climate variability and change. If we see an increase in precipitation within the Arctic region, will this coincide with a decrease or increase in the overall thickness of the sea ice and how will this effect rates of accretion and ablation over the annual cycle? The temporal and spatial dynamics in precipitation patterns also suggest that modeling this phenomenon would be less appealing than directly estimating snow thickness distributions remotely. The theoretical framework of both geophysical and thermodynamic effects on scattering and emission, as presented here, provide the framework for continued development of operational tools designed to estimate snow thickness classes over sea ice through an indication of the thermodynamic state of the snow sea ice system.

REFERENCES

- [1] R. Brown and P. Cote. "Interannual variability of landfast ice thickness in the Canadian high Arctic." *Arctic*, vol. 45, pp. 273-284, 1950.
- [2] G. Flato and R. D. Brown. "Sensitivity of landfast Arctic sea ice to changes in snow cover and climate as determined by a one-dimensional thermodynamic model." submitted for publication.
- [3] T. S. Ledley. "Snow on sea ice: Competing effects in shaping climate." *J. Geophys. Res.*, vol. 96, no. 17, pp. 195-208, 1991.
- [4] ———. "Variations in snow on sea ice: A mechanism for producing climate variations." *J. Geophys. Res.*, vol. 98, no. 10, pp. 401-410, 1993.
- [5] R. E. Moritz and D. K. Perovich, Eds., "Surface heat budget of the Arctic ocean science plan." Univ. Washington, Seattle. ARCSS/OAI Rep. 5, 1996, p. 64.
- [6] T. C. Grenfell and A. W. Lohanick. "Temporal variations of the microwave signatures of sea ice during the late spring and early summer near Mould Bay NWT." *J. Geophys. Res.*, vol. 90, pp. 5063-5074, 1985.
- [7] D. G. Barber, E. F. LeDrew, D. G. Flett, M. Shokr, and J. Falkingham. "Seasonal and diurnal variations in SAR signatures of sea ice." *IEEE Trans. Geosci. Remote Sensing*, vol. 30, pp. 638-642, May 1992.
- [8] D. P. Winebrenner, E. D. Nelson, R. Colony, and R. D. West. "Observation of melt onset on multi year Arctic sea ice using the ERS-1 synthetic aperture radar." *J. Geophys. Res.*, vol. 99, no. 22, pp. 425-441, 1994.
- [9] D. G. Barber and A. Thomas. "The influence of cloud on the radiation balance, physical properties, and microwave scattering of first-year and multiyear sea ice." *IEEE Trans. Geosci. Remote Sensing*, vol. 36, pp. 38-50, Jan. 1998.
- [10] S. G. Beaven, G. L. Lockhart, S. P. Gogineni, A. R. Hosseinmostafa, K. C. Jezek, A. J. Gow, D. K. Perovich, A. K. Fung, and S. Tjuatja. "Laboratory measurements of radar backscatter from bare and snow-covered saline ice sheets." *Int. J. Remote Sensing*, vol. 15, pp. 851-876, 1995.
- [11] V. I. Lytle, K. C. Jezek, S. Gogineni, and R. Hosseinmostafa. "Laboratory microwave backscatter from simulated sea ice with a snow cover."

- IEEE Trans. Geosci. Remote Sensing*, vol. 31, pp. 1009-1016, Nov. 1993.
- [12] T. G. Grenfell and G. A. Maykut. "The optical properties of ice and snow in the Arctic basin." *J. Glaciol.*, vol. 18, no. 80, pp. 445-463, 1977.
- [13] D. G. Barber, T. N. Papakyriakou, S. Shokr, and E. F. LeDrew. "An examination of the relationship between the spring period evolution of the scattering coefficients (σ°) and energy fluxes over landfast sea ice." *Int. J. Remote Sensing*, vol. 16, no. 17, pp. 3343-3363, 1995.
- [14] A. K. Fung, *Microwave Scattering and Emission Models and their Applications*. Norwood, MA: Artech House, 1994.
- [15] H. T. Chuah, S. Tjuatja, A. K. Fung, and J. W. Bredow. "A phase matrix for a dense discrete random medium: Evaluation of volume scattering coefficient." *IEEE Trans. Geosci. Remote Sensing*, vol. 34, pp. 1137-1143, Sept. 1996.
- [16] A. Stogryn. "The bilocal approximation for the electric field in strong fluctuation theory." *IEEE Trans. Antennas Propagat.*, vol. AP-31, pp. 985-986, June 1983.
- [17] D. G. Barber, S. P. Reddan, and E. F. LeDrew. "Statistical characterization of the geophysical and electrical properties of snow on landfast first-year sea ice." *J. Geophys. Res.*, vol. 100, pp. 2673-2686, 1995.
- [18] S. V. Nghiem, R. Kwok, S. H. Yueh, D. K. Perovich, A. J. Gow, C.-C. Hsu, K.-H. Ding, J. A. Kong, and T. C. Grenfell. "Diurnal thermal cycling effects on microwave signatures of thin sea ice." *IEEE Trans. Geosci. Remote Sensing*, vol. 36, pp. 111-125, Jan. 1998.
- [19] R. Kwok, S. V. Nghiem, S. Martin, D. P. Winebrenner, A. J. Gow, D. K. Perovich, C. T. Swift, D. G. Barber, K. M. Golden, and E. J. Knapp. "Laboratory measurements of sea ice: Connections to microwave remote sensing," this issue, pp. 1716-1730.
- [20] D. G. Barber and S. V. Nghiem. "On the estimation of snow thickness distributions over sea ice using active microwave scattering." *J. Geophys. Res.*, to be published.
- [21] S. V. Nghiem, R. Kwok, S. H. Yueh, A. J. Gow, D. K. Perovich, J. A. Kong, and C.-C. Hsu. "Evolution in polarimetric signatures of thin saline ice under constant growth." *Radio Sci.*, vol. 32, no. 1, pp. 127-151, 1997.
- [22] K. M. Golden, M. Cheney, K.-H. Ding, A. K. Fung, T. C. Grenfell, D. Isaacson, J. A. Kong, S. V. Nghiem, J. Sylvester, and D. P. Winebrenner. "Forward electromagnetic scattering models for sea ice." this issue, pp. 1655-1674.

David G. Barber, for a photograph and biography, see p. 50 of the January 1998 issue of this TRANSACTIONS.

A. K. Fung (S'60-M'66-SM'70-F'85), photograph and biography not available at the time of publication.

Thomas C. Grenfell (M'94-A'95), for a photograph and biography, see p. 124 of the January 1998 issue of this TRANSACTIONS.

Son V. Nghiem (M'86), for a photograph and biography, see p. 123 of the January 1998 issue of this TRANSACTIONS.

Robert G. Onstott (S'73-M'79), photograph and biography not available at the time of publication.

V. I. Lytle (M'95), photograph and biography not available at the time of publication.

Donald K. Perovich, for a photograph and biography, see p. 124 of the January 1998 issue of this TRANSACTIONS.

Anthony J. Gow, for a photograph and biography, see p. 124 of the January 1998 issue of this TRANSACTIONS.